journal

J. Am. Ceram. Soc., 96 [4] 1070–1076 (2013)
DOI: 10.1111/jace.12225

Enhanced Hydrothermal Resistance of Y-TZP Ceramics Through Colloidal Processing

E. Rayón,[‡,†] R. Moreno,[§] C. Alcázar,[§] M. D. Salvador,[‡] F. J. Manjón,[¶] E. Jiménez-Piqué,[‖] and L. LLanes[‖]

[‡]Instituto de Tecnología de Materiales, Universitat Politècnica de València, ES-46022 Valencia, Spain

[§]Instituto de Cerámica y Vidrio, CSIC, Kelsen 5, 28049 Madrid, Spain

[¶]Departament de Física Aplicada, Universitat Politècnica de València, Escuela Técnica Superior de Ingeniería del Diseño (ETSID), ES-46022 València, Spain

[‖]Depto de Ciencia de Materiales y Metalurgia, Universitat Politécnica de Catalunya, (ETSEIB) Av. Diagonal, 647 Barcelona, Spain

Two commercial zirconia powders with 3 mol% of yttria (TZ3YE and TZ3YS, labeled as ZE and ZS, respectively) supplied by Tosoh (Japan) were used for this study. Maximum colloidal stability for ZE was achieved by dispersing the powders in a mixture of water/ethanol of 90:10 (wt/wt) using a sonication probe. The rheological behavior of the suspensions was optimized in terms of solids content ranging from 20 to 33 vol% and sonication time (0–6 min), the best results being obtained after 2 min. ZS samples were prepared to a solids loading of 30 vol% in water dispersing with 2 min-sonication. Samples obtained by slip casting in plaster molds were used for dynamic sintering studies, and fully dense and nanostructured specimens were obtained at temperatures of 1300°C–1350°C (ZE samples) and 1400°C per 2 h (ZS samples). The Hardness (*H*) and Young's Modulus (*E*) properties of the specimens were studied by nanoindentation technique giving 17 and 250 GPa mean values for *H* and *E*, respectively. The specimens were then forced to a low-temperature degradation (LTD) treatment at 130°C for 240 h in steps of 60 h. Raman spectroscopy and nanoindentation results of hydrothermally treated samples showed the absence of transformation from tetragonal to monoclinic phase until 180 h whereas the mechanical properties maintained constant even at the sample surface. After 240 h of LTD, the monoclinic phase was detected on all specimens by Raman peaks centered at 180, 191, and 383 cm^{-1}. The nanoindentation study revealed an important loss of mechanical features reaching 10 and 175 GPa for *H* and *E*, respectively. In the case of the ZS specimens, no monoclinic phase is detected after 240 h of LTD treatment and no decay of *E* or *H* is detected. The free defect microstructure reached for the ZS specimen revealed a higher hydrothermal resistance so that it is concluded that the excellent behavior against thermal degradation is possible due to the large uniformity obtained by colloidal processing rather than the particle size of the starting powders.

I. Introduction

YTTRIA-STABILIZED tetragonal zirconia polycrystalline (Y-TZP) ceramics are used in a variety of structural and functional applications due to their high strength, high toughness, and good wear resistance over a wide temperature range.[1–3] Y-TZP belongs to the family of transformation-toughened ceramics,[4–6] whose main feature consists in a microstructure completely formed by metastable tetragonal grains at room temperature that can undergo transformation to monoclinic phase. This is associated with a volume increase of 3–4 vol%, which is the origin of a compressive stress field that operates inversely to the tensile stress that leads the crack and stops it. Factors affecting the phase transformation volume are as follows: the grain size of the tetragonal phase, the amount of stabilizer, and the restraining conditions.[7,8] Y-TZP materials are also used as a biomaterial, due to its excellent biocompatibility, for example, as dental replacements. However, low-temperature degradation (LTD) have hampered other applications, such as hip replacements,[9,10] and therefore it is one of the main limitations of the material. LTD, consist on the spontaneous transformation of the tetragonal phase into the monoclinic phase due to the presence of water even at room temperature, which causes microcracking of the material and loss of structural integrity.[11,12]

The degradation kinetics increases when the specimen is subjected to hydrothermal environments, which is the most usual situation in biomedical applications.[10,13,14]

Nowadays, the hydrothermal degradation can be reduced by either diminishing the grain size or by increasing the stabilizer content.[15–17] The porosity must be also avoided to reduce the degradation because it serves as migration path to introduce water inside the material. Furthermore, the geometrical shape of the grains is important as spherical grains should distribute the stresses more homogenously than faceted ones.

Nanostructured ceramics display a range of enhanced properties compared to those obtained with submicrometer counterparts.[18,19] However, the processing of nanopowders and its further densification to obtain dense nanostructures is difficult because of the strong tendency to agglomeration and spontaneous grain growth during sintering.[20,21] To overcome the densification problems, pressure-assisted sintering techniques have been used, such as hot-pressing,[2] and more recently, electric field-assisted sintering, also known as spark plasma sintering.[22,23] Other authors have investigated the possibility of using two-step sintering to achieve high densities while maintaining fine grain sizes.[24–26] To improve the lifetime and the reliability of the prostheses, the addition of a second phase such as carbon nanotubes is being investigated also.[27,28]

Commercial nanopowders easy to handle and with high reliability are readily available nowadays. However, a major

I. Reimanis—contributing editor

Manuscript No. 31515. Received June 4, 2012; approved January 16, 2013.
†Author to whom correspondence should be addressed. e-mail: emraen@upvnet.upv.es

concern for the production of nanostructured materials is the preparation of homogeneous, defect-free green bodies. In this sense, the colloidal approach has demonstrated its suitability for the production of uniform, dense green bulk bodies from nanopowders.[29–31] The use of nanopowders is necessary to maintain the nanostructure after sintering, as this is the only way to impede grain coarsening, which is the main responsible for the spontaneous degradation caused by tetragonal to monoclinic transformation (t → m), especially at low temperatures (in the range of 200°C–300°C).[32–37]

The aim of this work was to study the colloidal processing and the rheological behavior of concentrated suspensions of a mixture of commercial nano- and submicrometer-sized powders of Y-TZP to produce homogeneous green bodies with high density by slip casting. The obtained compacts were sintered to high density maintaining controlled grain size and the mechanical behavior of the sintered specimens before and after a forced LTD was studied by nanoindentation technique and characterized by Raman spectroscopy and FE-SEM observations.

II. Experimental Procedure

As starting materials, two different powders of zirconia containing 3 mol% of yttria were used (TZ3YS and TZ3YE; Tosoh, Japan). These powders and their subsequent samples will be labeled as ZS and ZE, respectively. Table I summarizes the physicochemical properties of these powders, which are supplied in the form of spherical granules with typical diameters of about 50 μm and below 100 nm for the ZS and the ZE, respectively. The measurement of the particle size distribution of ZS was performed using the laser diffraction technique (LD; Lasterisizer S, Malvern, UK) whereas the ZE powder required the use of dynamic light scattering (DLS; Zetasizer NanoZS, Malvern, UK). The redispersion in water for the measurements made the granules to redisperse, so that the measured average sizes for ZS and ZE were 0.9 and 0.4 μm, respectively. The specific surface area was determined using the single-point BET method [(Monosorb Surface Area Analyzer, MS-13; Quantachrome Corporation, Boynton Beach) after degassing at 150°C. The BET diameter was calculated from the measurements of particle size and surface area, giving values of 154 and 70 μm, for ZES and ZE, respectively. For comparison purposes, the agglomeration factor was calculated dividing the measured and the BET diameters, the resulting values being 2.6 and 13 for ZS and ZE, respectively. The last powder is much more agglomerated after redispersion in water than the former as a consequence of the lower particle size. The unit crystallite size was never reached with the soft dispersion procedure used herein. The density was measured by He-pycnometry, with a Multipycnometer; Quantachrome Co.], being 5.9 ± 0.2 g/cm^3 for both powders. The morphology of the as-received powders was observed by field-emission gun scanning electron microscopy (FE-SEM, Hitachi S-4700 type I, Hitachi, Tokyo, Japan), and transmission electron microscopy (TEM, H7100; Hitachi). The crystalline phases were identified by X-ray Diffraction (XRD; Bruker D8 Advance, Karlsruhe, Germany) and using the Garvie's approach the ratio of tetragonal phase (density = 6.07 g/cm^3, ASTM 83-113) and monoclinic phase (density = 5.82 g/cm^3, ASTM 37-1484), was found to be 68/32 and 82/18 for ZS and ZE powders, the resulting densities being 6.00 ± 0.1 g/cm^3. Differential thermal and thermogravimetric analysis of the as-received powder was carried out in air with a Netzsch STA-409 Thermoanalyzer (Selb, Germany), using alumina as the reference material, in the temperature range of 20°C–1500°C at a heating rate of 10°C/min.

ZE suspensions were prepared in a mixture of deionised water and ethanol (EtOH) with a weight ratio 90:10. The colloidal stability of ZE nanopowders was studied measuring the zeta potential as a function of pH using a Zetasizer NanoZS instrument (Malvern, UK), based in the laser Doppler velocimetry technique. Different dilutions were tested to measure the zeta potential with the best accuracy, which was reached for a concentration of 0.005 wt%, using KCl 0.01 M as inert electrolyte. The pH values were determined with a pH-meter (716 DMS Titrine, Metrohm, Switzerland) and were adjusted with HCl and KOH solutions (0.01 and 0.01 M). To improve the dispersion state, some sonication times were tested using an ultrasounds probe (UP 400S; dr. Hielscher GmbH, Germany). A sonication time of 2 min was used for the preparation of diluted suspensions for zeta potential measurements. Concentrated suspensions were prepared in water/EtOH to solids loadings of 20, 23, 28, and 33 vol% (i.e., 60, 65, 70, and 75 wt%, respectively).

Table I. Physicochemical Properties of the As-Received Powders

Powder	ZE	ZS
S_s (m^2/g)	14.5 ± 0.5	6.7 ± 0.5
Granule size, $d_{v,50}$ (μm)	0.9	0.4
Density (g/cm^3)	5.9 ± 0.3	5.9 ± 0.3
d_{BET} (nm)	70	154
Agglomeration factor (f_{agg})	~13	~2.6

The colloidal stability and rheological behavior of ZS suspensions has been studied elsewhere. In this work, reference ZS suspensions were prepared in water to a solids content of 30 vol% and a deflocculant content of 1.5 wt% on a dry solids basis. The deflocculant was a polyacrylic acid-based polyelectrolyte (Duramax D-3005; Rohm & Haas, Dow Chemical, Midland, MI) with an active matter content of 35%.

The rheological behavior of these suspensions was determined using a rheometer (Haake RS50; Thermo, Karlsruhe, Germany) operating at controlled shear rate by loading the shear rate from 0 to 1000 s^{-1} in 5 min, maintaining at 1000 s^{-1} for 1 min and uploading from 1000 to 0 in 5 min. The measurements were performed at 25°C using a double cone and plate system.

These suspensions were slip cast in plaster molds to obtain disks with 20 mm in thickness. Green densities were measured by Hg immersion after drying for 48 h. Sintering behavior was studied using green cast bodies through constant heating rate (heating and cooling rates 5°C/min) experiments up to 1600°C in a differential dilatometer with alumina rod (DI24; Adamel Lhomargy, Brie, France). Static sintering experiments for ZE samples were done to temperatures of 1350°C, 1300°C, and 1250°C with heating and cooling rates of 5°C/min. ZS reference samples were sintered at 1400°C. The annealing time selected was 2 h. The microstructures of diamond polished (down to 1 μm) samples were characterized by FE-SEM. The crystalline of the sintered specimens was determined by Raman spectroscopy using a LabRam HR UV microspectrometer (Horiba, Kyoto, Japan) (with a thermoelectrically cooled Charge-Coupled Device image sensor) from Horiba Jovin-Yvon (Longjumeau, France). Excitation was performed using the 532-nm laser line and focusing 10 mW of power on the sample with a 50x LWD objective, resulting in a resolution better than 3 cm^{-1}.

The Hardness (H) and Young's Modulus (E) of the sintered disks were analyzed using a nanoindenter (G-200 Agilent Technologies, Inc., Santa Clara, CA), before and after the hydrothermal degradation. Indentations were performed on the surface of samples previously polished with 0.25-μm diamond abrasives and using a calibrated diamond Berkovich tip. Tests were conducted using continuous stiffness measurement at 2 nm and 45 Hz harmonic oscillation. The hydrothermal treatment was performed at 130°C under steps of 60 h of aging in autoclave. The lapsed times treated were 60, 120, 180, and 240 h. After each degradation step, samples were nanoindented and analyzed by Raman spectrometer to reveal the maximum treatment time without visualize degradation effects.

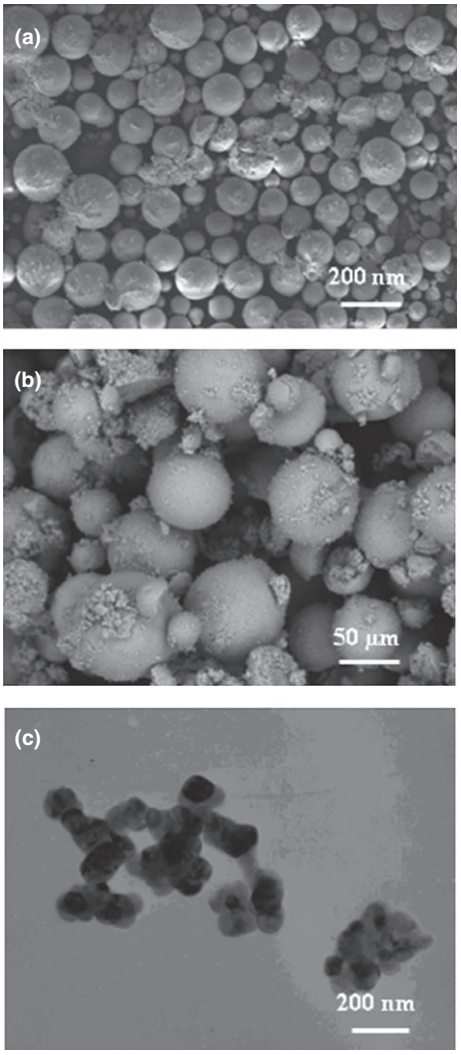

Fig. 1. Morphology of the starting TZ3YE powder (a), the TZ3YS powder (b), and a TEM picture of the smaller zirconia (c).

III. Results and Discussion

Figure 1 shows the morphology of the as-received powders observed by FE-SEM (Figs. 1 (a) and (b)] and a TEM picture of the ZE zirconia [Fig. 1(c)]. The powders are supplied in the form of spherical granules with submicronic (<50 μm) and nanometric size (<100 nm), respectively. TEM pictures of ZE powder show that primary particles have small agglomerates formed by several units.

Suspensions of the reference zirconia powder (ZS) showed an isoelectric point of around pH 6. The addition of 1.5 wt% PAA shifted down the IEP to pH 2.5. Concentrated suspensions were prepared in water to 30 vol% solids with 1.5 wt% of PAA mixing with a sonicator for 2 min. These suspensions were slightly shear thinning and had a viscosity of 13 mPa·s at a shear rate of 1000 s^{-1}. No further studies were done with this powder as it is better known in the bibliography.

The stability of the suspensions of ZE in water/EtOH is shown in Fig. 2. The isoelectric point occurs at pH 4.3, in the same range of other studies, but the zeta potential values are rather small. However, suspensions maintained stable for long times.

This is confirmed for concentrated suspensions which were stable against time. Figure 3 shows the flow curves of suspensions prepared to solids loading of 20, 23, 28, and 33 vol% solids and different sonication times. A sonication time of 2 min was necessary to provide maximum stability for any

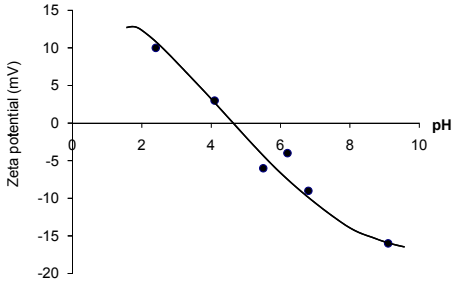

Fig. 2. Variation in zeta potential with pH for suspensions prepared in water:ethanol (90:10).

solids content. Suspensions prepared by mechanical mixing without sonication had some thixotropy. Optimized suspensions, i.e., those prepared with sonication for 2 min, had different rheological behavior depending on the solids loading. Less concentrated suspensions behave as nearly Newtonian or presented some shear thickening at high shear rate. The suspension with 28 vol% solids was slightly shear thinning and the most concentrated one presented some thixotropy. This variation is related to the increase in viscosity with solids loading. Figure 4 shows the variation in viscosity with sonication time for all solids loadings for a shear rate of 100 s^{-1}.

These suspensions were slip cast and the dried specimens were used for dynamic sintering and isothermal sintering tests. Table II shows the green density of the cast bodies, which tend to increase with solids content from 55% to 56.8% of theoretical density. Figure 5 shows the dilatometry of a cast specimen, in which it can be observed that early sintering necks start to form at 1000°C, maximum sintering rate is reached at 1200°C and at 1400°C a plateau is reached, thus suggesting that sintering process cannot progress anymore. Figure 6 shows the FE-SEM images of the samples sintered at 1250°C, 1300°C, and 1350°C before the hydrothermal degradation. The materials seem to have full density for all temperatures (Table III), and there are no apparent defects. The particle size is in the nanometer size region; although an increase is clearly observed for 1350°C thus demonstrating that this temperature is too high for sintering. In Fig. 6, the SEM microstructure of the reference sample ZS sintered at 1400°C is also shown for comparison purposes. It can be observed that the sample has reached full density and grain size is nearly the same as the starting particle size (grain size ranging from 100 to 300 nm).

Figure 7 shows the profile of hardness and Young's modulus as a function of indentation depth for the specimens obtained at the three selected sintering temperatures. These results evidence that no important differences were found for differently sintered specimens, giving average values of 17 and 250 GPa for H and E, respectively, which demonstrates that nearly full density is achieved even at the lowest sintering temperature. These results are in good agreement with previously reported H and E data for this material.[38,39]

After 60 h of LTD treatment, the aspect of all samples was equal than as-prepared without change of their coloration appearance and without observable microcracks. In this sense, Raman peaks observed at 147 and 256 cm^{-1} corroborated that only tetragonal phase was maintained even after the LTD treatment for all specimens. These features were maintained until 240 h of LTD treatment. After this lapsed time, samples were extracted from the autoclave with a yellowish coloration. Figure 8 (a) shows a comparison of the Raman spectra of LTD treatment (240 h) and as-sintered ZE samples. As observed, Raman spectra revealed the characteristic monoclinic double peak centered at 181–190 cm^{-1} for all sintered temperatures corroborating that t → m degradation by LTD treatment was reached after 240 h. Similarly,

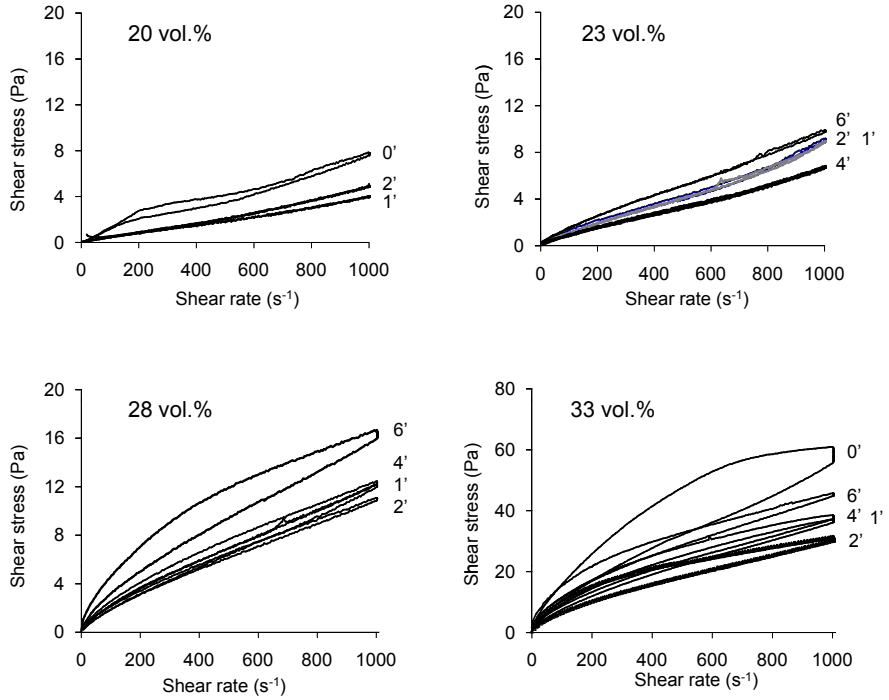

Fig. 3. Flow curves of suspensions prepared to solids loadings of 20, 23, 28, and 33 vol% and different sonication times.

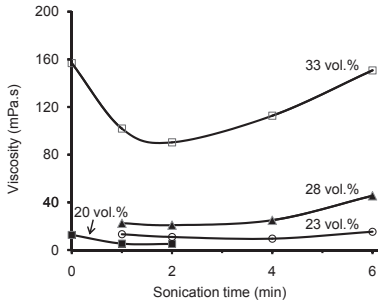

Fig. 4. Variation in viscosity with sonication time for suspensions prepared to different solids loadings (shear rate, 100 s^{-1}).

Table II. Green Densities of Cast Bodies

Solids content (wt%)	Solids content (vol%)	Density (g/cm^3)	Relative density (% TD)
60	20	3.22	55.0
65	23	3.27	55.9
70	28	3.06	52.3
75	33	3.33	56.8

Table III. Densities of Sintered Materials

Temperature	Density (g/cm^3)	Relative density (% TD)
1250°C	5.87	97.1
1300°C	6.02	98.9
1350°C	6.06	99.6

Fig. 8(b) shows the Raman spectra of the ZS samples, before and after degradation tests. The t → m transformation is not observed in this material even after 240-h thermal degradation, thus suggesting that the colloidal processing itself allows the preparation of zirconia materials with extreme resistance to thermal degradation. The fact that the ZS powder gives

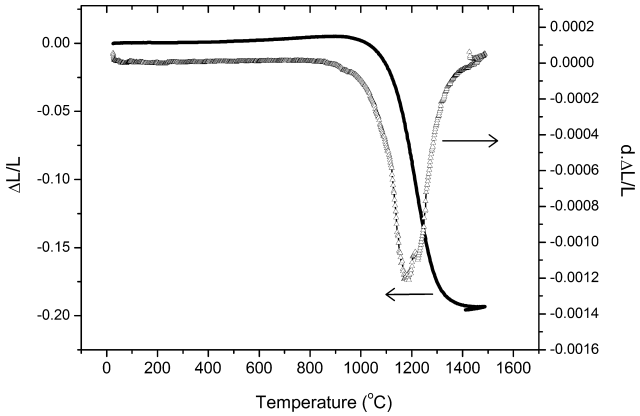

Fig. 5. Shrinkage and derivative curves of a cast specimen sintered at 1500°C.

largest resistance than the nanometric ZE must be related to the higher density and the absence of defects in the microstructure of the former, and the presence of some isolated defects and pores in the last.

Nevertheless, a thin degraded layer containing monoclinic phase on the ZS specimen may have not been detected due to the resolution of the Raman technique. Thus, the complete absence of the monoclinic phase on the specimen is not assured by these results. The FE-SEM images and nanoindentation results display this phenomenon. We think that any possible difference from the hydrothermal degradation resistance as a function of the sintering temperature might be found studying the crystalline and mechanical properties in depth profiles. Accordingly, Fig. 9 shows the *H* and *E* profiles acquired after 240 h of LTD for the ZE samples. It can be observed that they have constant values from the surface until 2 μm penetration depth reached in the experiment, indicating that t→m transformation achieves several micrometers in depth. The values recorded for *H* and *E* were 10 and 175 GPa, respectively, agreeing with previous reported values on monoclinic zirconia.[40]

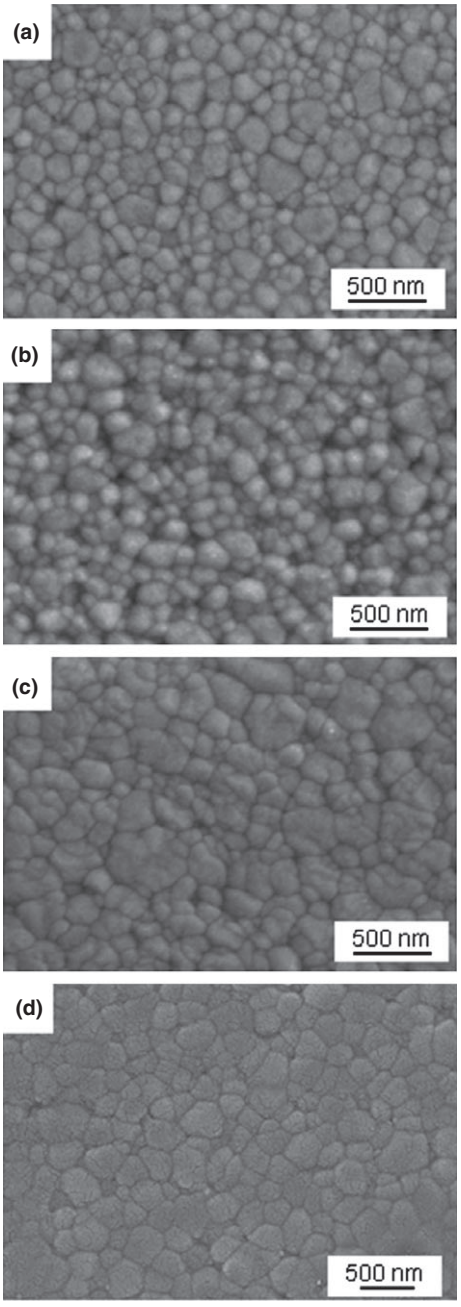

Fig. 6. FE-SEM microstructures of TZ3YE specimens sintered at 1250°C (a), 1300°C (b), and 1350°C (c), and the microsctructure of the TZ3YS sintered at 1400°C (d).

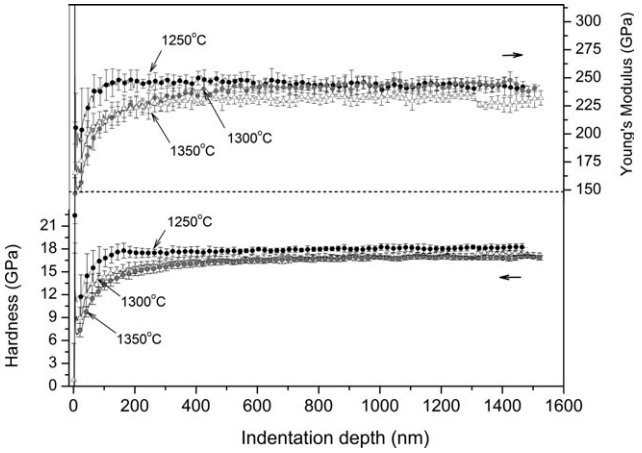

Fig. 7. Average and standard deviation of the Hardness and Young's Modulus curves acquired by nanoindentation for TZ3YE specimens sintered at 1250°C, 1300°C, and 1350°C.

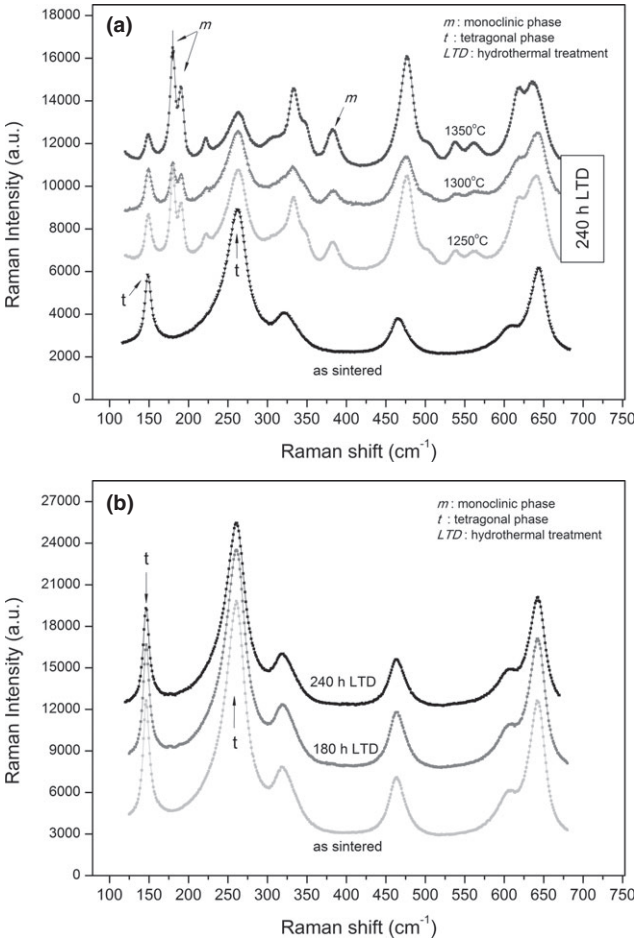

Fig. 8. Raman spectra acquired before and after LTD treatment (a) on a TZ3YE and (b) TZ3YS specimen.

The results of nanoindentation tests performed on ZS samples before and after LTD for 240-h treatment are shown in Fig. 10. These results show that values of E and H maintain constant after the extreme treatment of 240 h, even better than observed for the nanosized powder, which maintain stable until 180 h but then degradation occurs for 240 h as detected by the decrease in mechanical properties.

Figures 11 (a) and (b) display representative FE-SEM cross-section images of the top degraded layer observed for degraded specimens after LTD at 240 h treatment. A lot of grooves could be observed on the ZE specimen as a consequence of released grains probably in the polishing procedure for approximately 20 μm in depth from the surface. For the ZS specimen the affected zone was also observable but thinner than in previous case. This sample showed a nonhomogeneous degraded zone that varies from 250 nm to 1.75 μm thick. The affected zone width agrees with nanoindentation profile results. This means that the volumetric expansion produced by the t → m transformation generates microcracks in the grains boundaries leading to a cohesion fall between them. The fast propagation in depth of the t → m reaction once the degradation began was due to the autocatalytic character of this reaction.[38] We have avoided the use of this observed "degraded layer depth" to compare the degradation resistance between specimens because the width of this layers were not uniformity affected on sample probably due to holders used into the autoclave.

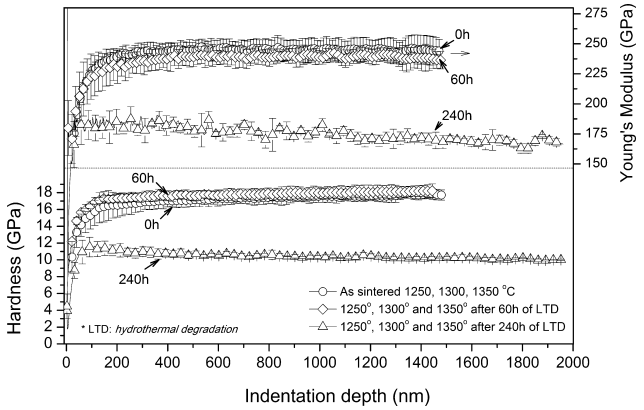

Fig. 9. Average of the Hardness and Young's Modulus curves acquired by nanoindentation for TZ3YE specimens sintered at 1250°C, 1300°C, and 1350°C, and after 60 h of hydrothermal degradation and after 240 h.

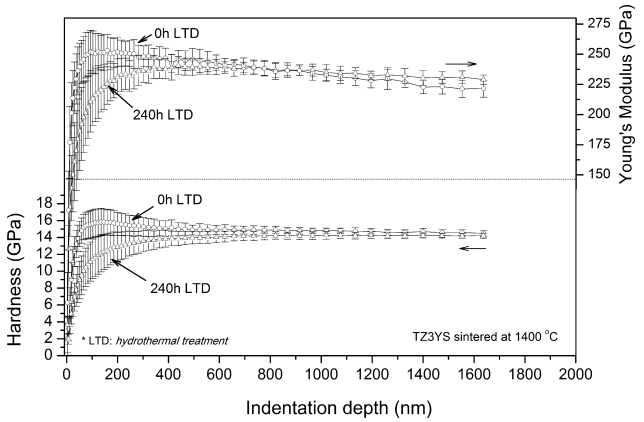

Fig. 10. Average of the Hardness and Young's Modulus profiles for TZ3YS specimen sintered at 1400°C and after 240 h of hydrothermal degradation.

Although a limit for the stability against LTD was established, it was as high as 240 h, these results corroborate that the stability of the tetragonal phase was higher than that reported in other studies.[39,40] This raise in the hydrothermal resistance is explained by the maintenance of grain sizes and by the high density reached during green processing. It is known that the smaller the grain size the larger the hydrothermal resistance,[41] but the results shown in this work demonstrate that the absence of defects reached with the ZS powder is a major issue to obtain the excellent properties reported herein, whereas the ZE powder that would lead to enhanced properties has a lower resistance to degradation, probably due to the presence of small, isolated defects. This implies that by means of a cheap and single slip casting and the subsequent conventional sintering procedures, it is possible to make nanostructured zirconia materials with complex geometries and with enhanced lifetime features.

IV. Conclusions

Concentrated suspensions of commercially available nanosized Y-TZP were prepared to solids loadings ranging from 20 to 33 vol% in a water/ethanol mixture (90:10) mixing with an UP. The better slip casting performance was achieved for a solids content of 28 vol% and 3-min sonication. Green densities of cast bodies ranged between 55% and 57% of theoretical density. Near to theoretical density was achieved by conventional sintering at temperatures of 1250°C, 1300°C, and 1350°C, although the last presented

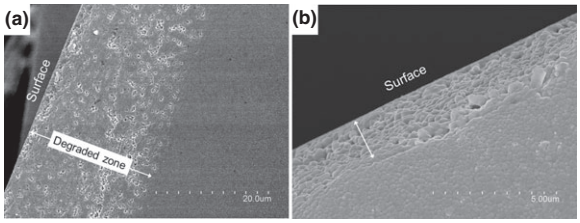

Fig. 11. FE-SEM cross-section image of a TZ3YE (a) and TZ3YS (b) specimen hydrothermally degraded during 240 h.

some grain coarsening. The Raman spectra and FE-SEM images showed that tetragonal phase was the unique phase detected and a nanostructure with grains below the 250 nm was maintained. Nanoindentation tests led to hardness and Young's modulus values of 17 and 250 GPa, respectively, for any sintering temperature within the studied range. The reference ZS specimen sintered at 1400°C revealed a high-density microstructure without observable defects with a grain size distribution similar than ZE samples.

Hydrothermal treatments were then performed on sintered specimens using an autoclave at 130°C and 60, 120,180, and 240 h of aging. Only after 240 h, the monoclinic phase was detected on the ZE specimen by the double Raman peak centered at 181–190 cm^{-1} for all sintered temperatures. The t → m transformation led to a loss of the mechanical features. The nanoindentation hardness and modulus were 10 and 175 GPa, respectively. The FE-SEM images of the cap degraded layer displayed an affected zone of approximately 20 μm in depth. The ZS specimen showed a higher hydrothermal degradation resistance than previous sample prepared with nanometer powder. Raman technique was not capable to detect monoclinic phase after 240 h of hydrothermal treatment, although FE-SEM images revealed a nonhomogeneous thin cap degraded layer. These results agreed with nanoindentation Hardness and Modulus profiles showing loss of mechanical response below 600 nm depth.

Acknowledgments

This work has been supported by Spanish Ministry of Science and Innovation (Projects MAT2009-14144-C03-02, MAT2009-14369-C02-01, and MAT2008-03398). Authors thank Prof. M. Anglada for helpful comments and discussion. R Moreno thanks the Universidad Politécnica de Valencia for the concession of a grant in the frame of its Program of Support to R+D (PAID-02-11, R-1752). We also wish to acknowledge Rut Benavente for her excellent technical support.

References

[1]R. C. Garvie, "Structural Applications of ZrO_2-Bearing Materials"; pp. 465–78 in *Zirconia II. Adv. Ceram.*, Vol **12**, Edited by N. Claussen, M. Ruhle and A. H. Heuer. American Ceramic Society, Westerville, OH, 1984.

[2]B. Basu, J. Vleugels, and O. van der Biest, "Toughening Tailoring of Yttria-Doped Zirconia Ceramics," *Mater. Sci. Eng., A*, **380** [1–2] 215–21 (2004).

[3]A. G. Evans, "Perspective on the Development of High-Toughness Ceramics," *J. Am. Ceram. Soc.*, **73**, 187–206 (1990).

[4]N. Claussen, "Microstructural Design of Zirconia-Toughened Ceramics (ZTC)"; pp. 325–51 in *Zirconia II., Adv. Ceram.*, Vol **12**, Edited by N. Claussen, M. Rühle and A. H. Heuer. American Ceramic Society, Westerville, OH, 1984.

[5]M. Ruhle and A. H. Heuer, "Phase Transformations in ZrO_2 Containing Ceramics: II, The Martensitic Reaction in t-ZrO_2"; pp. 14–32 in *Zirconia II., Adv. Ceram.*, Vol **12**, Edited by N. Claussen, M. Ruhle and A. H. Heuer. American Ceramic Society, Westerville, OH, 1984.

[6]A. H. de Aza, J. Chevalier, and G. Fantozzi, "Slow-Crack-Behaviour of Zirconia-Toughened Alumina Ceramics Processed by Different Methods," *J. Am. Ceram. Soc.*, **86** [1] 115–20 (2003).

[7]R. H. J. Hannik, P. M. Kelly, and B. C. Muddle, "Transformation Toughening in Zirconia Containing Ceramics," *J. Am. Ceram. Soc.*, **83** [3] 461–87 (2000).

[8]B. Basu, J. Vleugels, and O. van der Biest, "Transformation Behaviour of Tetragonal Zirconia. Role of Dopant Content and Distribution," *Mater. Sci. Eng., A*, **366** [2] 338–47 (2004).

[9]C. Piconi, W. Burger, H. G. Richter, A. Cittadini, G. Maccauro, V. Covacci, N. Bruzzese, G. A. Ricci, and E. Marmo, "Y-TZP Ceramics for Artificial Joint Replacements," *Biomaterials*, **19**, 1489–94 (1998).

[10]J. Chevalier, "What Future for Zirconia as a Biomaterial?" *Biomaterials*, **27**, 535–43 (2006).
[11]E. Jiménez-Piqué, A. Ramos, J. A. Muñoz-Tabares, A. Hatton, F. Soldera, F. Mücklich, and M. Anglada, "Focused ion Beam Tomography of Zirconia Degraded Under Hydrothermal Conditions," *J. Eur. Ceram. Soc.*, **32**, 2129–36 (2012).
[12]A. Muñoz-Tabares, E. Jimenez-Pique, and M. Anglada, "Subsurface Evaluation of Hydrothermal Degradation of Zirconia," *Acta Mater.*, **59**, 473–84 (2011).
[13]J. L. Masonis, R. B. Bourne, M. D. Ries, R. W. McCalden, A. Salehi, and D. C. Kelman, "Zirconia Femoral Head Fractures: A Clinical and Retrieval Analysis," *J. Arthroplasty*, **19** [7] 898–905 (2004).
[14]J. Chevalier, L. Gremillard, A. V. Virkar, and D. R. Clarke, "The Tetragonal-Monoclinic Transformation in Zirconia: Lessons Learned and Future Trends," *J. Am. Ceram. Soc.*, **92** [9] 1901–20 (2009).
[15]F. F. Lange, "Transformation Toughening - Part 1 Size Effects Associated With the Thermodynamics of Constrained Transformations," *J. Mater. Sci.*, **17** [1] 225–34 (1982).
[16]A. G. Evans, N. Burlingame, M. Drory, and W. M. Kriven, "Martensitic Transformations in Zirconia-Particle Size Effects and Toughening," *Acta Metall.*, **29** [2] 447–56 (1981).
[17]S. Shukla and S. Seal, "Mechanisms of Room Temperature Metastable Tetragonal Phase Stabilization in Zirconia," *Int. Mater. Rev.*, **50**, 45–64 (2005).
[18]M. Mayo, "Processing of Nanocrystalline Ceramics From Ultrafine Particles," *Int. Mater. Rev.*, **41**, 85–115 (1996).
[19]M. A. Meyers, A. Mishra, and D. J. Benso, "Mechanical Properties of Nanocrystalline Materials," *Prog. Mater Sci.*, **51**, 427–556 (2006).
[20]J. G. P. Binner and B. Vaidhyanathan, "Processing of Bulk Nanostructured Ceramics," *J. Eur. Ceram. Soc.*, **28**, 1329–33 (2008).
[21]J. R. Groza, "Sintering of Nanocrystalline Powder," *Int. J. Powder Metall*, **35** [7] 59–66 (1999).
[22]D. Yang, R. Raj, and H. Conrad, "Enhanced Sintering Rate of Zirconia (3Y-TZP) Through the Effect of a Weak dc Electric Field on Grain Growth," *J. Am. Ceram. Soc.*, **93** [10] 2935–7 (2010).
[23]J. Langer, M. J. Hoffmann, and O. Guillon, "Electric Field Assisted Sintering in Comparison With the hot Pressing of Yttria Stabilized Zirconia," *J. Am. Ceram. Soc.*, **94** [1] 24–31 (2011).
[24]C. Robert, F. Ansart, C. Deloget, M. Gaudon, and A. Rousset, "Dense Yttria Stabilized Zirconia: Sintering and Microstructure," *Ceram. Int.*, **29** [2] 151–8 (2003).
[25]X. H. Wang, P. L. Chen, and I. W. Chen, "Two-Step Sintering of Ceramics With Constant Grain Size: I: Y_2O_3," *J. Am. Ceram. Soc.*, **89** [2] 431–7 (2006).
[26]J. Binner, K. Annapoorani, A. Paul, I. Santacruz, and B. Vaidhyanathan, "Dense Nanostructured Zirconia by two Stage Conventional/Hybrid Microwave Sintering," *J. Eur. Ceram. Soc.*, **28**, 973–7 (2008).
[27]W. A. Curtin and B. W. Sheldon, "CNT-Reinforced Ceramics and Metals," *Mater. Today*, **7**, 44–9 (2004).
[28]N. Garmendia, I. Santacruz, R. Moreno, and I. Obieta, "Zirconia-MWCNT Nanocomposites for Biomedical Applications Obtained by Colloidal Processing," *J. Mater. Sci. - Mater. Med.*, **21**, 1445–51 (2010).
[29]O. Vasylkiv and Y. Sakka, "Synthesis and Colloidal Processing of Zirconia Nanopowder," *J. Am. Ceram. Soc.*, **84** [11] 2489–94 (2001).
[30]I. Santacruz, K. Anapoorani, and J. G. P. Binner, "Preparation of High Solids Content Nanozirconia Suspensions," *J. Am. Ceram. Soc.*, **91** [2] 398–405 (2008).
[31]B. P. C. Ragupathy and J. G. P. Binner, "Spray Granulation of Nanometric Zirconia Particles," *J. Am. Ceram. Soc.*, **94** [1] 42–8 (2011).
[32]K. Kobayashi, H. Kuwajima, and T. Masaki, "Phase Change and Mechanical Properties of ZrO_2-Y_2O_3 Solid Electrolyte After Ageing," *Solid State Ionics*, **3–4**, 489–93 (1981).
[33]S. Tsugio, O. Shiro, E. Tadashi, and S. Masahiko, "Transformation of Yttria-Doped Tetragonal ZrO_2 Polycristals by Annealing Under Controlled Humidity Conditions," *J. Am. Ceram. Soc.*, **68** [12] 320–2 (1985).
[34]S. Tsugio and S. Masahiko, "Transformation of Yttria-Doped Tetragonal ZrO_2 Polycrystals by Annealing in Water," *J. Am. Ceram. Soc.*, **68** [6] 356–9 (1985).
[35]S. Guicciardi, T. Shimazono, and G. Pezzotti, "Nanoindentation Characterization of sub-Micrometric Y-TZP Ceramics," *Adv. Eng. Mater.*, **8** [10] 994–7 (2006).
[36]J. A. Munoz-Tabares and M. Anglada, "Hydrothermal Degradation of Ground 3Y-TZP," *J. Eur. Ceram. Soc.*, **32**, 325–33 (2012).
[37]A. Paul, B. Vaidhyanathan, and J. G. P. Binner, "Hydrothermal Aging Behavior of Nanocrystalline Y-TZP Ceramics," *J. Am. Ceram. Soc.*, **94** [7] 2146–52 (2011).
[38]Y. Gaillard, M. Anglada, and E. Jimenez-Pique, "Nanoindentation of Yttria-Doped Zirconia: Effect of Crystallographic Structure on Deformation Mechanisms," *J. Mater. Res.*, **24** [3] 719–27 (2009).
[39]M. Cattani-Lorente, S. S. Scherrer, P. Ammann, M. Jobin, and H. W. A. Wiskott, "Low Temperature Degradation of a Y-TZP Dental Ceramic," *Acta Biomater.*, **7**, 858–65 (2011).
[40]Y. Gaillard, E. Jiménez-Piqué, F. Soldera, F. Mücklich, and M. Anglada, "Quantification of Hydrothermal Degradation in Zirconia by Nanoindentation," *Acta Mater.*, **56**, 4206–16 (2008).
[41]R. Chintapalli, A. Mestra, F. G. Marro, H. Yan, M. Reece, and M. Anglada, "Stability of Nanocrystalline Spark Plasma Sintered 3Y-TZP," *Materials*, **3**, 800–14 (2010). □